Indium oxide "rods in dots" nanostructures

G. Q. Ding, W. Z. Shen,[a] M. J. Zheng, and Z. B. Zhou
Laboratory of Condensed Matter Spectroscopy and Opto-Electronic Physics, Department of Physics, Shanghai Jiao Tong University, 1954 Hua Shan Road, Shanghai 200030, China

(Received 25 January 2006; accepted 22 June 2006; published online 9 August 2006)

The authors have demonstrated a special indium oxide (In_2O_3) "rods in dots" nanostructure with high nanorod sheet density of over 10^{12} cm^{-2}. The approach has been realized through depositing controllable individual In_2O_3 nanorods in both number and shape within a single porous alumina membrane (PAM) nanochannel under radio frequency magnetron sputtering. The authors further discussed in detail effects of the PAM configurations (pore diameter and thickness) and sputtering conditions (substrate temperature and argon pressure) on the formation of the In_2O_3 nanostructure. © *2006 American Institute of Physics*. [DOI: 10.1063/1.2335665]

Nanostructured materials have unusual physical and chemical properties different from those of bulk materials and are promising for the fabrication of nanodevices.[1–3] In particular, nanodot arrays fabricated on semiconductor substrates with high density are of great interest for technological applications due to their unique size dependent properties and easy integration into functional quantum devices.[4–6] Current e-beam writing machines can readily write thousands of nanodots with great accuracy and without extraneous efforts. However, the process would take extraordinary amount of time to write hundreds of millions of nanodots.[7] The developed dip-pen nanolithography has the same shortcomings although highly ordered nanodot arrays can also be obtained using atomic force microscope cantilevers dipped in certain solutions as pens.[8,9]

To fabricate highly ordered large area nanodot arrays, the anodic porous alumina membranes (PAMs) are ideal templates, which have controllable nanopore arrays with interpore spacing ranging from 50 to 500 nm, pore diameter from 20 to 250 nm, and membrane thickness from 0.1 to 200 μm.[10–12] The general fabrication process of nanodot arrays by the aid of PAMs is schematically shown in Figs. 1(a)–1(c). The nanodots are deposited on the substrate through the PAM nanochannels with only one nanodot in a single PAM nanochannel. The nanodot array can be realized after the PAM is removed in chemical solution. Metals, such as Fe,[4] Au,[6] Ni,[13] and Co,[14] and semiconductor nanodots, such as GaAs,[5] Si,[13,15] and ZnO,[16] have been fabricated using PAMs as templates.

Nevertheless, it should be noted that the density of the yielded nanodot arrays is the same as that of PAM nanopores and limited to $\sim 10^{11}$ pores/cm^2. One way to improve the nanodot sheet density is to increase the nanopore density of PAMs, which is restricted by the PAM fabrication. Another way is to deposit multiple nanounits in a single PAM nanochannel. Masuda *et al.*[6] have demonstrated two or three metal nanoparticles in a single PAM nanochannel through twice shadowed evaporation of various materials. For quantum device application, it is expected to deposit more nanounits in a single PAM nanochannel for further increase of the sheet density. In this letter, we report on the realization of nanodot arrays with controllable nanorods in a single nanodot under a magnetron sputtering in conjunction with the PAM technique, as shown schematically in Figs. 1(d)–1(f).

The demonstration of this kind of "rods in dots" nanostructure has been carried out on indium oxide (In_2O_3), which has a direct band gap of ~3.7 eV and has been widely used in solar cells, organic light emitting diodes, gas sensors, and windows that absorb sunlight.[17–19] In_2O_3 can also be one of the most attractive conductive oxides for field emission because of its convenience of *n*-type doping, relatively low electron affinity, high chemical inertness, and sputter resistance. The fact that many kinds of nanoscale In_2O_3 microstructures, such as nanoparticles,[20] nanowires,[21] nanochains,[22] nanofibers,[23] nanobelts,[24] nanotubes,[25] nanopyramids,[26] and [27] have been synthesized under different growth methods forms the base for the realization of In_2O_3 nanostructures with "nanounits in nanodots" by the aid of the PAMs.

The freestanding ultrathin PAMs were washed and transferred onto Si substrates for the In_2O_3 deposition. A parallel plate rf magnetron sputtering system was used to grow In_2O_3 layer. The In_2O_3 sputtering target was hot-pressed oxide ceramic (90 wt % In_2O_3 and 10 wt % SnO_2 with purity of 99.99%), and sputtering gas was 99.999% argon. The working chamber was pumped lower than 1×10^{-3} Pa before sputtering and the space between target and substrate was

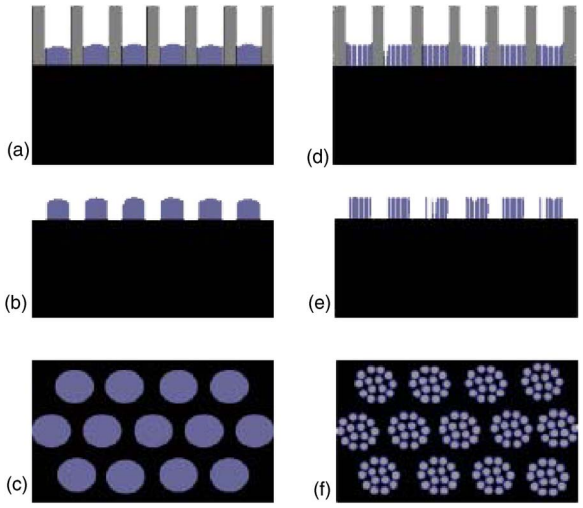

FIG. 1. Schematic diagrams of (a) one nanodot deposited in a single PAM nanochannel, together with (b) cross-sectional and (c) top views of the nanodot array after the removal of the PAM; (d) many nanorods deposited through a single PAM nanochannel, together with (e) cross-sectional and (f) top views of the rods in dots nanostructure after the removal of the PAM.

[a]Author to whom correspondence should be addressed; electronic mail: wzshen@sjtu.edu.cn

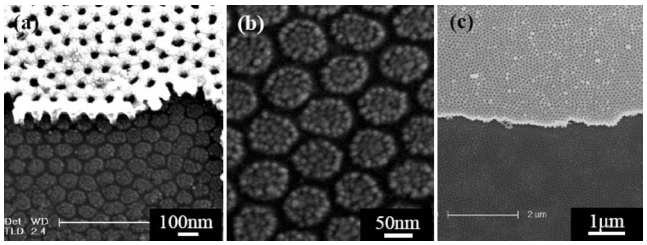

FIG. 2. FESEM images of (a) In_2O_3 nanodot array after partial PAM was removed, (b) enlarged nanodot array with ~30 nanorods in every nanodot, and (c) large area In_2O_3 nanodot array.

fixed at a short distance of 2.6 cm. During deposition, the substrate temperature and working gas pressure were kept at 180 °C and 0.5 Pa, respectively. The morphology and microstructure of the yielded In_2O_3 nanopores were characterized by field emission scanning electron microscope (FESEM) (Philips XL30FEG), x-ray diffraction (XRD) (Bruker D8 Advance system with Cu $K\alpha_1$ radiation of 0.154 056 nm), and high-resolution transmission electron microscope (HRTEM) (JEOL JEM-2100F).

Figure 2(a) displays the morphology of the In_2O_3 nanodot array after partially removing the PAM (~150 nm in thickness) with the In_2O_3 nanopores on top of it. It is found that the yielded In_2O_3 nanodots are with a diameter of ~85 nm, in good agreement with the original PAM pore diameter of ~90 nm. Enlarged FESEM top view image [Fig. 2(b)] of the In_2O_3 nanodots demonstrates that every nanodot is composed of ~30 individual nanorods with the average diameter of ~13 nm. This fabricated rods in dots nanostructure remarkably improves the sheet density to reach over 10^{12} cm^{-2} in nanomaterials fabricated through the PAM templates, ten times of the general nanodots via PAMs.[4–6,13–16] Furthermore, profiting from the large-scale fabrication of the PAMs,[10,11] the area of the synthesized In_2O_3 rods in dots nanostructure can be over several square centimeters. The low magnification FESEM image in Fig. 2(c) displays an area over 7×5 μm^2 with partially unremoved PAM.

The realization of many In_2O_3 nanorods within a single PAM channel benefits from both sputtering technique for In_2O_3 and PAM confining effect. Under the magnetron sputtering, many kinds of nanoscale microstructures can be synthesized due to controllable adatom mobility and different growth rates along various directions. The three-zone model, proposed by Movchan and Demchishin[28] and later developed by Thornton,[29] can describe well the sputtered microstructures with nanocolumnar, tapered, and fibrous grains. Metal[28] (such as Ni, Ti, and W) and oxide [such as Al_2O_3,[28] ZrO_2,[28] ZnO,[30] MgO,[31] and In_2O_3 (Ref. 32)] nanorods have been realized under appropriate argon pressures and T/T_m values (where T is the substrate temperature and T_m is the material melting point). We have deposited In_2O_3 under different conditions, and found that In_2O_3 tends to have highly ordered nanorod shape under an appropriate temperature of 180 °C and relatively low argon pressure of 0.5 Pa. The PAM confining effect leads to the independent In_2O_3 nanorods in every nanochannel. Without the PAMs, the In_2O_3 nanorods will compose a continuous film on the Si substrate.

The microstructure of the fabricated In_2O_3 nanorods was characterized by HRTEM and XRD. Figure 3(a) displays the HRTEM image of two individual In_2O_3 nanorods with the average diameter ~13 nm and height ~50 nm. The inset in Fig. 3(a) displays the HRTEM image of several individual

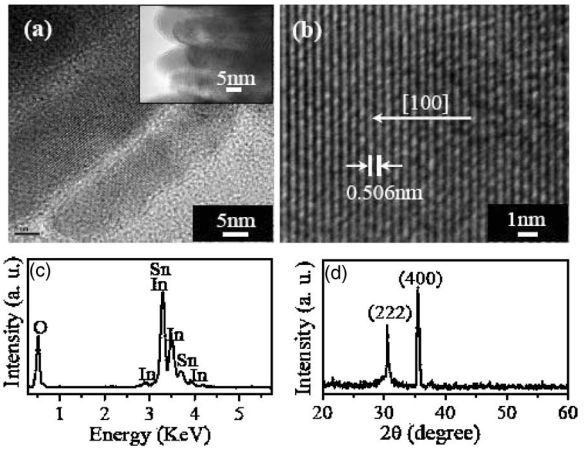

FIG. 3. [(a) and (b)] HRTEM images of the In_2O_3 nanorods, and (c) EDX and (d) XRD spectra of the In_2O_3 nanodot array. The inset in (a) is the HRTEM image of several In_2O_3 nanorods.

In_2O_3 nanorods with a cross-sectional view. According to both the SEM and TEM results, these In_2O_3 nanorods are independent, vertical to the substrates, and parallel to each other. The lattice fringes in nanorods confirm that every In_2O_3 nanorod is single crystalline. Figure 3(b) reveals the 0.506 nm lattice spacing of the cubic In_2O_3 plane (200) and the [100] nanorod growth orientation, and this kind of preferable growth is consistent with the synthesis mechanism of other In_2O_3 nanostructures, such as nanowires,[22] nanofibers,[24] and nanobelts.[25] The energy dispersive spectroscopy (EDS) analysis [Fig. 3(c)] during HRTEM observation confirms that there are three elements in the nanopores, i.e., indium, tin, and oxygen, with an approximate atomic indium to tin ratio of ~14:1. The doping of tin in In_2O_3 decreases the resistivity, which is beneficial to the application of highly ordered In_2O_3 nanostructures in nanoelectronic devices. The two diffraction peaks in XRD spectrum [Fig. 3(d)] can be attributed to (222) and (400) planes of the cubic In_2O_3 structure of Mn_2O_3 (I) type with a cell constant of 1.012 nm. The XRD results coincide well with the above demonstrated preferable [100] growth orientation of In_2O_3 nanorods through HRTEM images.

It should be noted that photoluminescence (PL) of In_2O_3 normally originates from the near-band-edge[20] and defect-related emissions.[25,26] However, it is difficult to detect the weak near-band-edge emissions of pure and good-quality In_2O_3, since bulk In_2O_3 cannot emit light at room temperature.[33] There are only two papers in the literature[20] reporting the near-band-edge emissions in synthesized In_2O_3 nanoparticles with small sizes, where a mass of such nanoparticles can be used during the PL measurement. In contrast, our present ultrathin (~50 nm) samples have only fixed and limited nanorods. The small amount of the In_2O_3 nanorods leads to the difficulty in observing the weak near-band-edge emissions. Strong defect-related emissions are always related to the amorphous In_2O_3 or oxygen vacancies, and have been widely observed in not-so-good In_2O_3 samples.[25,26] The experimental fact that we cannot detect any defect-related emissions in our In_2O_3 nanorods confirms the good quality of our present In_2O_3 nanorods, consistent with the HRTEM and XRD observations.

Since the fabricated In_2O_3 rods in dots nanostructure originates from both confining effect of the PAMs and control of sputtered In_2O_3 nanoscale microstructures, the mor-

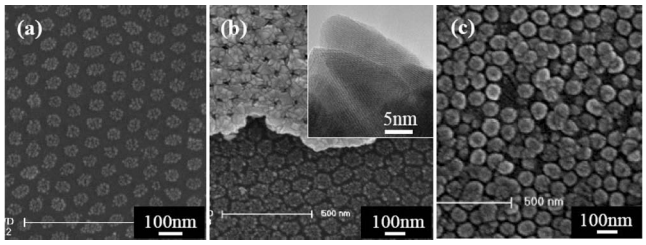

FIG. 4. FESEM images of (a) In_2O_3 nanodot array deposited through the PAM with a thickness of 300 nm and pore diameter of 90 nm, (b) In_2O_3 nanodot array deposited under a high growth temperature of 250 °C with the HRTEM image of the yielded nanorods shown in the inset, and (c) In_2O_3 nanodot array deposited under a high argon pressure of 2.0 Pa.

phology of the In_2O_3 nanostructure, including the number of nanorods in every nanodot, is sensitive to either the PAM configurations or sputtering conditions. The pore diameter and thickness of PAMs are key facts during the In_2O_3 deposition. When the PAM thickness is about 300 nm, the size of the In_2O_3 nanodots reduces to only ~50 nm with only ~15 nanorods in each nanodot under the same pore diameter (~90 nm) PAMs, as shown in Fig. 4(a), while no nanodots or nanorods were found under small pore diameter (~50 nm) ones. With the further increase in the PAM thickness of over 500 nm, no In_2O_3 nanodots can be found on the Si substrates after the PAMs are removed, no matter what the pore diameters are. Large pore size and thin PAM will help the deposition of In_2O_3 nanodots through the PAM nanochannels, and the thinner the PAMs are, the more regular the obtained In_2O_3 nanodots are.

In addition to the PAM configurations, the sputtering conditions, especially the growth temperature and argon pressure, will also play key roles in the fabrication of In_2O_3 rods in dots nanostructure. Figure 4(b) shows the FESEM morphology of the sputtered In_2O_3 under the same growth conditions as in Fig. 2 (including the same PAM) except for a growth temperature of 250 °C. It is found that the deposited In_2O_3 microstructure transforms from nanorods into faceted grains under high temperatures, as shown in the inset HRTEM image of Fig. 4(b). At the same time, the size of the nanorods increases to ~20 nm, resulting in the decrease of nanorod number (~20) in each nanodot. In fact, low growth temperature is helpful to obtain ordered nanorods in the sputtering technique,[30,31] except for poor crystallization of the sputtered In_2O_3 under too low temperature.[34]

The argon pressure is usually kept in the range of 0.3–5.0 Pa during sputtering oxides.[29–32] High argon pressure will bring the scattering of energetic reflected species, which does harm to the preferable growth of In_2O_3 nanorods. Figure 4(c) displays the top view FESEM image of In_2O_3 nanorods sputtered under 2.0 Pa (the others are the same as in Fig. 2), where it is hard to find individual nanorods in each nanodot due to the immersion of nanorods into single nanodots as a result of scattering effect under high argon pressures. The deposition rate also increases with the enhanced argon pressure, which leads to the irregularity of the fabricated In_2O_3 nanodot array.

Finally, it should be noted that low growth temperature and argon pressure are helpful to obtain independent In_2O_3 nanorods. The nanorods, fabricated under 180 °C and 0.5 Pa, are all separate and single crystalline, as shown in Figs. 2(b) and 3(a). In contrast, the nanorods, sputtered under a high growth temperature of 250 °C and argon pressure of 2.0 Pa, have somewhat fused into polycrystalline nanodots, as shown in Figs. 4(b) and 4(c). Nevertheless, the microstructure and distribution of the In_2O_3 nanorods are not related to the thickness and pore diameter of PAMs.

This work was supported in part by the National Natural Science Foundation of China, PCSIRT, and the Shanghai Major Project Nos. 03DJ14003 and 05DJ14003.

[1] S. Kara, M. R. Pafall, W. H. Rippard, T. J. Silva, S. E. Russek, and J. A. Katine, Nature (London) **437**, 389 (2005).
[2] M. Law, D. J. Sirbuly, J. C. Johnson, J. Goldberger, R. J. Saykally, and P. D. Yang, Science **305**, 1269 (2004).
[3] Z. H. Zhong, D. L. Wang, Y. Cui, M. W. Bockrath, and C. M. Lieber, Science **302**, 1377 (2003).
[4] K. Liu, J. Nogués, C. Leighton, H. Masuda, K. Nishio, I. V. Roshchin, and I. K. Schuller, Appl. Phys. Lett. **81**, 4434 (2002).
[5] X. Y. Mei, M. Blumin, D. Kim, Z. H. Wu, and H. E. Ruda, J. Cryst. Growth **251**, 253 (2003).
[6] H. Masuda, K. Yasui, and K. Nishio, Adv. Mater. (Weinheim, Ger.) **14**, 1031 (2000).
[7] Y. W. Su, C. S. Wu, C. C. Chen, and C. D. Chen, Adv. Mater. (Weinheim, Ger.) **15**, 49 (2003).
[8] P. E. Sheehan, L. J. Whitman, W. P. King, and B. A. Nelson, Appl. Phys. Lett. **85**, 1589 (2004).
[9] R. D. Piner, J. Zhu, F. Xu, S. H. Hong, and C. A. Mirkin, Science **283**, 661 (1999).
[10] H. Chik and J. M. Xu, Mater. Sci. Eng., R. **43**, 103 (2004).
[11] K. Nielsch, J. Choi, K. Schwirn, R. B. Wehrspon, and U. Gösele, Nano Lett. **2**, 677 (2002).
[12] G. Q. Ding, M. J. Zheng, W. L. Xu, and W. Z. Shen, Nanotechnology **16**, 1285 (2005).
[13] J. Liang, H. Chik, A. Yin, and J. M. Xu, J. Appl. Phys. **91**, 2544 (2002).
[14] R. Zhu, Y. T. Pang, Y. S. Feng, G. H. Fu, Y. Li, and L. D. Zhang, Chem. Phys. Lett. **368**, 696 (2003).
[15] G. Q. Ding, W. Z. Shen, M. J. Zheng, W. L. Xu, Y. L. He, and Q. X. Guo, J. Cryst. Growth **283**, 339 (2005).
[16] W. L. Xu, M. J. Zheng, G. Q. Ding, and W. Z. Shen, Chem. Phys. Lett. **411**, 37 (2005).
[17] A. Gutarra, A. Azens, B. Stjerna, and C. G. Granqvist, Appl. Phys. Lett. **64**, 1064 (1994).
[18] C. C. Wu, C. I. Wu, J. C. Sturm, and A. Kahn, Appl. Phys. Lett. **70**, 1348 (1997).
[19] T. Takada, K. Suzukik, and M. Nakane, Sens. Actuators B **13**, 404 (1993).
[20] W. S. Seo, H. H. Jo, K. Lee, and J. T. Park, Adv. Mater. (Weinheim, Ger.) **15**, 795 (2003); A. Murali, A. Barve, V. J. Leppert, S. H. Risbud, I. M. Kennedy, and H. W. H. Lee, Nano Lett. **1**, 287 (2002).
[21] P. Nguyen, H. T. Ng, J. Kong, A. M. Cassell, R. Quinn, J. Li, J. Han, M. McNeil, and M. Meyyappan, Nano Lett. **3**, 925 (2003).
[22] J. Y. Lao, J. Y. Huang, D. Z. Wang, and Z. F. Ren, Adv. Mater. (Weinheim, Ger.) **16**, 65 (2004).
[23] C. H. Liang, G. W. Meng, Y. Lei, F. Phillipp, and L. D. Zhang, Adv. Mater. (Weinheim, Ger.) **13**, 1330 (2001).
[24] Z. W. Pan, Z. R. Dai, and Z. L. Wang, Science **291**, 1947 (2001).
[25] Y. B. Li, Y. Bando, and D. Golberg, Adv. Mater. (Weinheim, Ger.) **15**, 581 (2003).
[26] P. Guha, S. Kar, and S. Chaudhuri, Appl. Phys. Lett. **85**, 3851 (2004).
[27] G. Q. Ding, W. Z. Shen, M. J. Zheng, and Z. B. Zhou, Nanotechnology **17**, 2590 (2006).
[28] B. A. Movchan and A. V. Demchishin, Phys. Met. Metallogr. **28**, 83 (1969).
[29] J. A. Thornton, J. Vac. Sci. Technol. **11**, 666 (1974).
[30] E. Mirica, G. Kowach, P. Evans, and H. Du, Cryst. Growth Des. **4**, 147 (2004).
[31] P. Pinto, J. I. Poothra, S. C. Purandare, S. P. Pai, C. P. D'Souza, D. Kumar, and M. Sharon, J. Vac. Sci. Technol. A **9**, 2670 (1991).
[32] A. K. Kulkarni, K. H. Schulz, T. S. Lim, and M. Khan, Thin Solid Films **308–309**, 1 (1997).
[33] Y. Ohhata, F. Shinoki, and S. Yoshida, Thin Solid Films **59**, 255 (1979).
[34] Y. Hoshi and T. Kiyomura, Thin Solid Films **411**, 36 (2002).